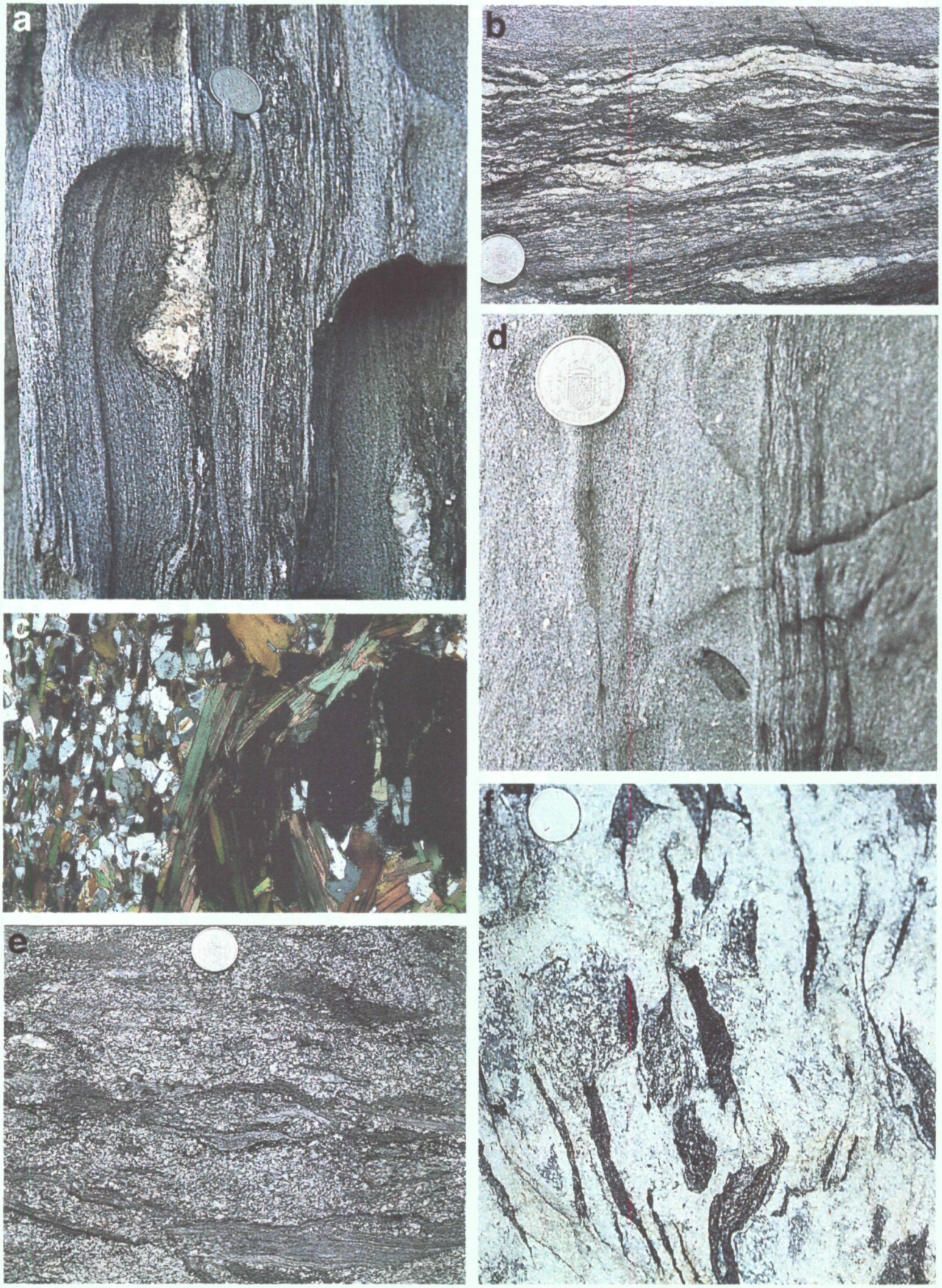

Fig. 23. (a): Migmatite schist with quartzofeldspathic segregations, Tudela. (b): Stromatic migmatite. (c): Microphotograph of a migmatite schist. The neosome (at the right) is coarser grained and contains garnet (Width of view 7 mm. CPL). (d): Contact between a psammitic schist and a foliation-parallel granodiorite vein (nebulitic migmatite). (e): Migmatite resulting from the injection of a granodioritic magma. (f): Migmatite resulting from the injection of a leucogranitic magma. Location of (b), (c), (d), (e) and (f): Punta dels Farallons migmatite complex.

Rock	migmatite schist	melano-some
SiO_2	67,71	46,14
TiO_2	0,78	1,13
Al_2O_3	14,03	22,73
Fe_2O_3	6,11	11,81
MnO		0,18
MgO	3,09	5,35
CaO	1,4	2,56
Na_2O	2,73	3,66
K_2O	3,19	4,37
P_2O_5		0,08
H_2O	0,88	1,33
Total	99,92	99,35

Table 4. Chemical composition of migmatites from the Punta dels Farallons migmatite complex, after Druguet et al. (1995).

Migmatites formed by the injection of magma: At the outcrop scale, they constitute a mixture between granitoids and metasediments, and correspond to the arterite type defined by Mehnert (1968). They display schlieren, agmatic and raft structures (Fig. 23e, f). A garnet-rich rim usually exists between the schists and the granitoid bodies, involving biotite loss in the surrounding area.

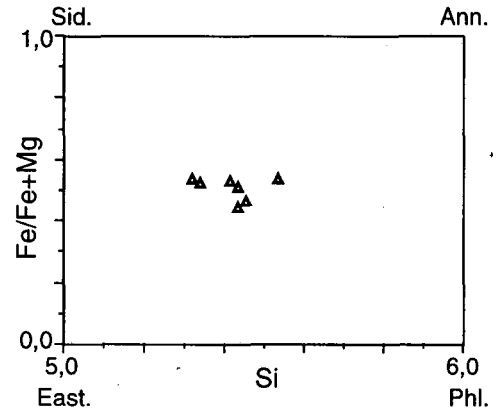

Fig. 24. Fe/Fe+Mg versus Si composition of biotites of migmatites from the Punta dels Farallons migmatite complex (after Druguet 1992).

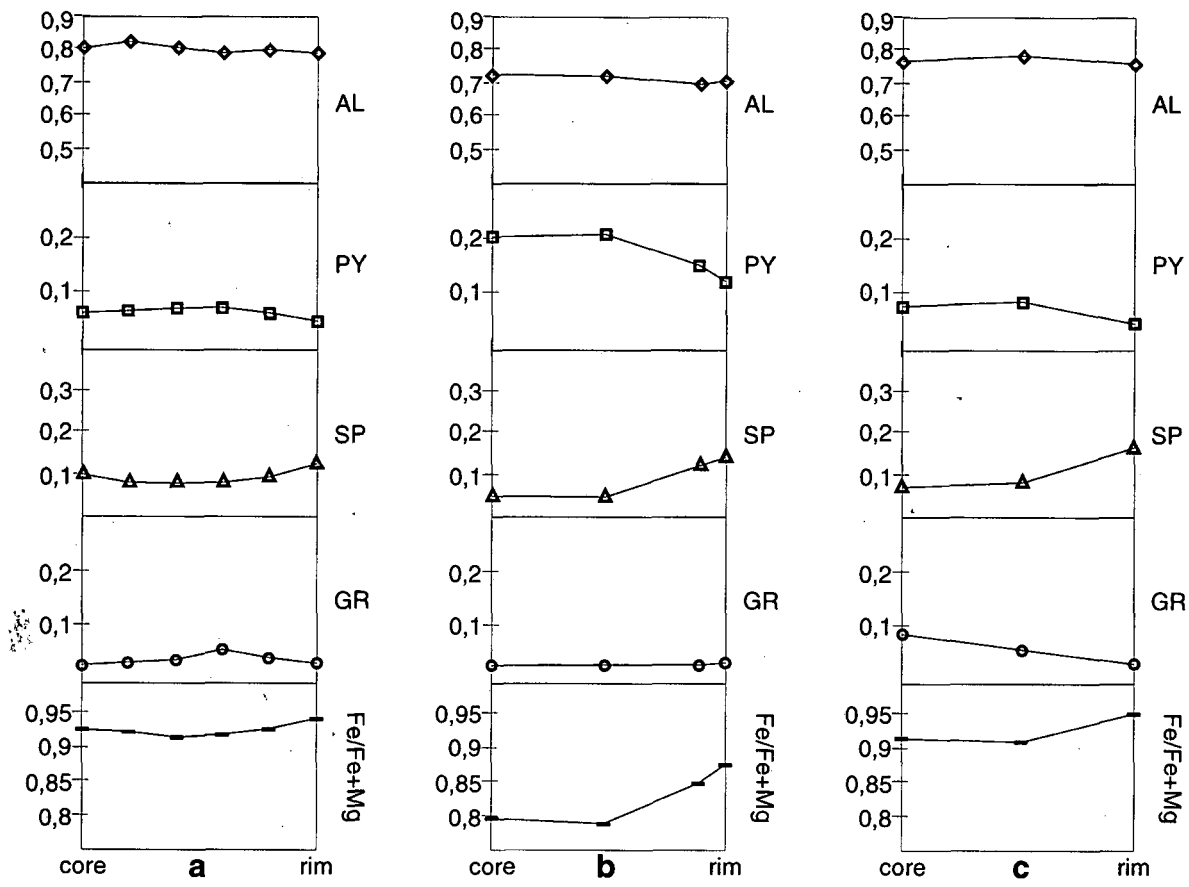

Fig. 25. Compositional diagrams of garnets from the Punta dels Farallons migmatite complex. (a): migmatite schist. (b) melanosome. (c): intrusive granite. AL, PY, SP and GR are the almandine, pyrope, spessartine and grossular components.

Magmatic rocks

The magmatic rocks in the Punta dels Farallons migmatite complex (Fig. 11) range from small bodies of hornblende-rich quartz gabbros and quartz-diorites to garnet-bearing peraluminous leucogranites and pegmatites. They are heterogeneous in composition, the more acid types containing xenoliths or enclaves of the more basic types. They occur as small bodies (up to 150 m x 60 m), which may be lensoid-shaped or have fold-like forms. However, the more acid units usually occur as veins or dykes. Compositional banding and schlieren structures are common. As it will be seen in section 5.2, they show different degrees of deformation, recorded as magmatic and solid-state fabrics.

Major element compositions of characteristic granitoid types are shown in Table 5.

The magmatic rocks have been divided into two associations (Druguet et al., 1995). From older to younger, these are a) a cafemic association, which forms a calc-alkaline sequence comprising hornblende quartz gabbros, quartz diorites, tonalites, granodiorites and granites and b) a later peraluminous association, which may be anatectic in origin and comprises leucogranites and pegmatites. Some veins and dykes of trondhjemitic composition are also peraluminic, but occupy an intermediate position between the two associations.

Hornblende quartz gabbros

The hornblende quartz gabbros (or bojites according to the classification of Hughes 1982 and Le Maître 1989) are the most basic rocks in the complex. Two types have been distinguished. Type 1 occurs either as enclaves within granitoids or as a discontinuous sub-vertical dyke which extends eastwards from the migmatite complex. Best outcrops are located out of the migmatite complex in Cala Sardina (Fig. 26). Type 2 (quartz gabbros with lesser Mg content) form small intrusive bodies displaying irregular and diffuse contacts with quartz diorites. They are dark-coloured, homogeneous and fine to medium-grained, and consist of calcic plagioclase (bytownite in type 1 and labradorite in type 2), amphibole (magnesio-hornblende to actinolitic hornblende), biotite (Fe/Fe+Mg~0.4, Fig. 27) and quartz (Fig. 28). Common accessories are sphene, apatite, zircon and opaque minerals.

Rock	Qb1		Qb2	Qd-e	Qd		Tonalites			Grd		Trond	Lgrt	
SiO_2	53,1	54,8	52,1	49,6	53,4	53,5	53,7	57,5	61,2	65,9	66,8	71,5	74,5	75,1
TiO_2	0,7	0,79	2,21	2,15	1,68	0,81	1,83	0,89	0,91	0,61	0,75	0,24	0,15	0,14
Al_2O_3	15,5	17,1	18,2	18,9	18,5	20,4	18,9	18,6	17,6	17,2	15,8	15,9	13,7	13,8
Fe_2O_3	10,5	8,63	10,8	11,9	9,6	10,9	9,08	9,87	6,7	3,77	4,97	2,33	1,21	1,06
MnO	0,22	0,21	0,17	0,15	0,16	0,25	0,15	0,12	0,11			0,04		
MgO	7,19	6,17	3,28	3,2	2,68	1,39	2,88	1,51	2,38	1,5	1,66	0,6	0,38	0,18
CaO	8,67	8,59	7,23	7,59	6,56	4,63	5,62	4,62	4,39	3,54	3,06	2,88	1,22	0,88
Na_2O	0,81	0,59	2,74	3,6	3,82	4,1	2,77	3,4	2,92	4,44	3,12	4,46	3,4	3,27
K_2O	1,55	1,93	1,67	2,29	2,29	2,33	2,8	2,26	2,49	1,7	2,81	1,07	4,39	5,09
P_2O_5	0,09	0,13	0,38	0,46	0,33	0,39	0,72	0,4	0,2			0,04		
H_2O	0,8	0,87	0,42	0,36	0,57	0,42	0,86	0,66	0,76	0,74	0,6	0,63	0,54	0,34
Total	99,1	99,8	99,1	100	99,5	99,1	99,3	99,8	99,6	99,4	99,5	99,7	99,4	99,8

Table 5. Chemical composition of granitoids from the Punta dels Farallons migmatite complex. Qb1: quartz gabbros type 1; Qb2: quartz gabbros type 2; Qd-e: quartz diorite enclaves; Grd: granodiorites; Trond: trondhjemites; Lgrt: leucogranites. After Druguet et al. (1995).

Fig. 26. Dyke of quartz gabbro at Cala Sardina.

Quartz diorites, tonalites, granodiorites and granites

Both quartz diorites and tonalites can be divided in several types: those with biotite + amphibole, those with biotite only and those with biotite + almandine garnet (Fig. 28 and Fig. 29b). Plagioclase crystals are zonated, with a calcic core (An_{50-40}). Amphibole composition varies between magnesio-hornblende and ferro-tschermakite. The Fe/Fe+Mg ratio of biotites is about 0.5-0.6 (Fig. 27). Clinozoisite is relatively abundant and ilmenite and sphene are common accessories.

A progressive depletion in mafic minerals is observed towards the granodioritic and granitic types (Fig. 28), although garnet is locally abundant as almandine + quartz clusters or as schlierens. The garnet-rich facies occurs in the boundaries with the enclosing migmatite schists. Garnet forms 2-6 mm sized subhedral crystals with a weak retrograde zonation (Fig. 25).

Xenoliths of the enclosing metasediments and microgranular enclaves are rather frequent in these intermediate rocks (Fig. 29a).

Medium grained leucocratic rocks

These are peraluminous in composition and occur as veins and dykes between 5 cm and 50 m in width. They are not restricted to the migmatite area: they are also present in the sillimanite zone, forming a 500 m wide aureole, where they coexist with pegmatites. The occurrence of leucogranites in the migmatite and sillimanite zones has been observed in other Hercynian settings as the Trois Seigneurs massif (Wickham 1987). Laterally, some of the leucocratic veins can develop into coarse-grained pegmatites.

The most representative leucocratic rock type consists of biotite-muscovite leucogranite (Fig. 28). These rocks consist of quartz, plagioclase (oligoclase-albite), K-feldspar, biotite (Fe/Fe+Mg~0.65, Fig. 27) and muscovite. The local presence of variable amounts of almandine give place to garnet-rich leucogranites. Accessories are sillimanite, zircon, tourmaline and opaque minerals. Less abundant are small veins or dykes of biotite leucotonalites, trondhjemitic in composition.

Pegmatites

These rocks are specially abundant in the migmatite complexes. Since they have been already described, this reference is to point out that pegmatites are the latest intrusions in the study area, so that they are injected into the whole set of migmatite rocks and granitoid bodies.

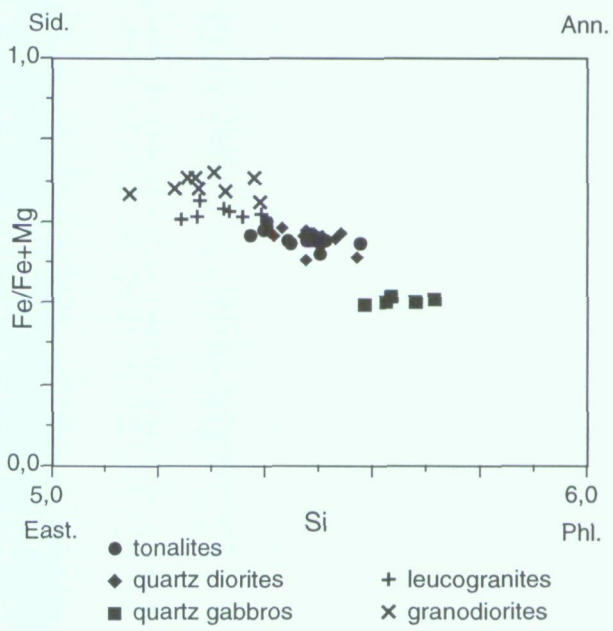

Fig. 27. Fe/Fe+Mg versus Si composition of biotites of different granitoids from the Punta dels Farallons migmatite complex (after Druguet 1992).

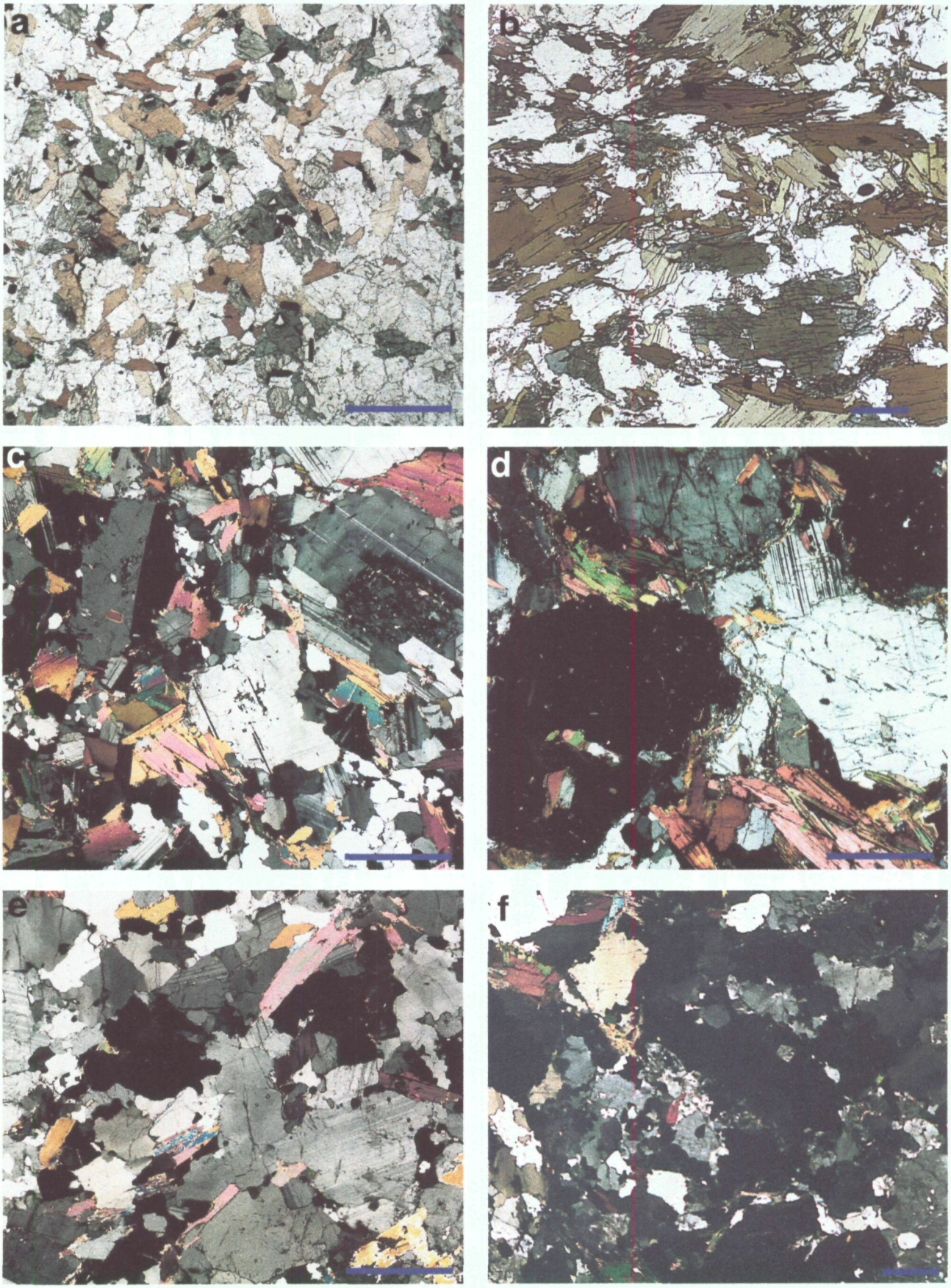

Fig. 28. Microphotographs of granitoids from the Punta dels Farallons migmatite complex. Scale bar = 1 mm. (a): Hornblende quartz gabbro (type II). PPL. (b): Quartz diorite with amphibole and biotite. PPL. (c): Biotite tonalite. CPL. (d): Tonalite with garnet and biotite. CPL. (e): Granodiorite. CPL. (f): leucogranite. CPL.

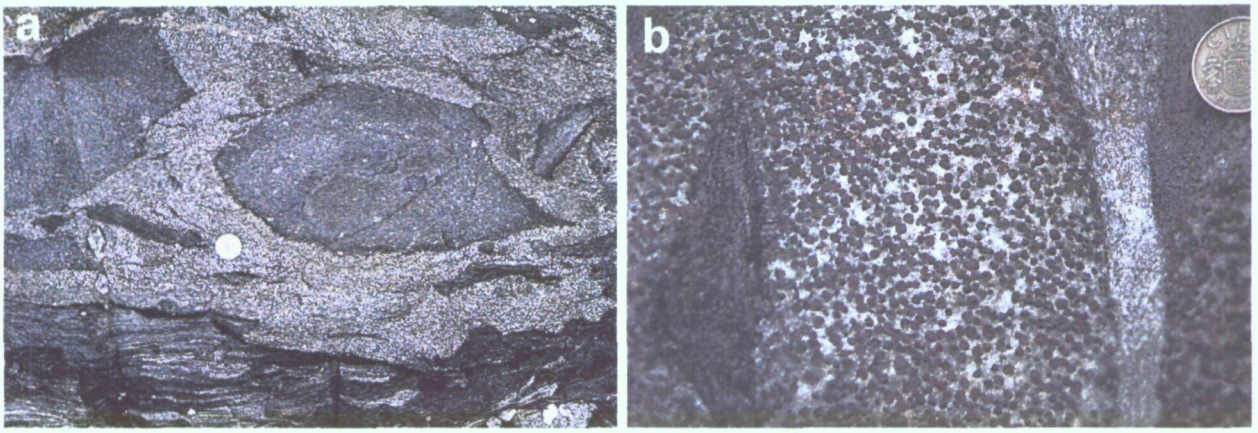

Fig. 29. Field photographs of granitoids of the Punta dels Farallons migmatite complex. (a): Microdioritic enclaves in a small granodiorite body. (b): Garnet-rich tonalite with a metasedimentary enclave. It is intruded by a leucogranite vein in the right side of the photograph.

3.3.3. A DISCUSSION ON THE MAGMATIC HISTORY

Prograde metamorphism in the Cap de Creus might have evolved towards partial melting of the metasediments, giving rise to local migmatization. The minimum PT conditions would be of 670°C and 3.3 Kbar or 2.5 Kbar for metastable equilibria, according to Grant (1985). Anatexis at lower crustal levels than those observable in outcrop might have produced the rocks of the peraluminous association (leucogranites and pegmatites). These magmas could derive from partial melting of the pelitic metasediments, in consistence with data obtained by Damm et al. (1992).

Some granitoids of the calc-alkaline sequence (granodiorites and biotite tonalites) could be the result of greywackic schists mobilization, since their compositional correspondence (Fig. 30). However, mantle-derived magmas with different degrees of crustal contamination may have originated the majority of the small intrusive granitoid bodies. In this way, the less differentiated hornblende quartz gabbros would represent the less contaminated extreme. Hence, Complex processes of magma mixing or hybridization could also be involved. In addition, the presence of these gabbroids and dioritoids suggests the possibility of them inducing a local anatexis on the nearby metasediments. Then, the thermal flow related to such intrusions would have produced an additional heating effect, so that the water-saturated sillimanite schists would have reached the melting curve. This would explain satisfactorily the nature of the migmatites, restricted to few small areas around the granitoid intrusions. Therefore, the ascent of intermediate-basic magmas and the induced local anatexis are considered to be the prevailing processes in the development of the migmatite complexes. Moreover, the presence of calc-alkaline intrusive rocks in areas of medium to high grade metamorphism allows to relate both processes, metamorphism and magmatism, in a way that might explain the low pressure-high thermal gradient metamorphism in the Cap de Creus.

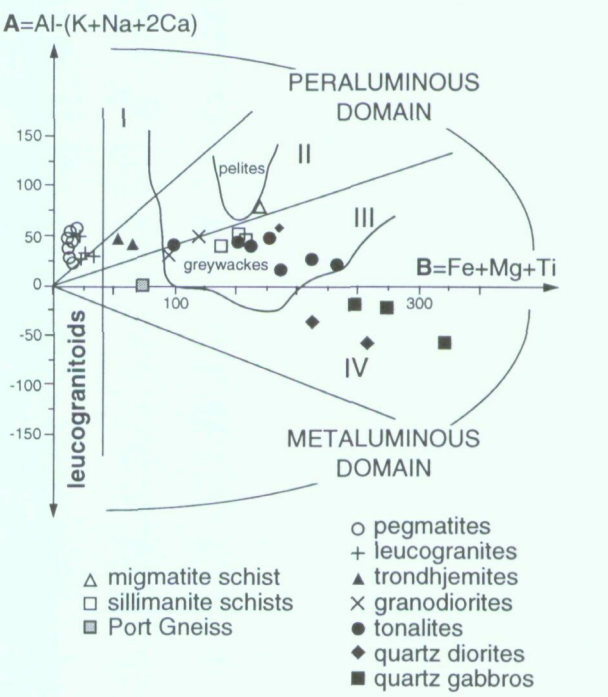

Fig. 30. AB plot of the migmatite complex rocks (after Debon & Le Fort (1983)). I: peraluminous rocks with ms>bt (in volume). II: peraluminous rocks with bt>ms. III: peraluminous rocks with bt only. IV: metaluminous rocks with bt+ amph ± px.

3.4. P-T ESTIMATES

Few quantitative data on temperature and pressure conditions of metamorphism have been obtained from the study area. The main results are exposed in Fig. 31. In geothermometry, the following equilibria have been used: garnet-biotite (Hodges & Spear 1982), biotite-muscovite (Hoisch 1989), biotite-chlorite (Dickenson & Hewitt 1986), biotite-tourmaline (Colopietro & Friberg 1987) and Plagioclase-K-feldspar (Stormer 1975, Stormer & Whitney 1985).

Pressure conditions have only been estimated for the sillimanite-muscovite (Coll de ses Portes) and migmatite (Punta dels Farallons) zones, by using the garnet-biotite-plagioclase geobarometer of Hodges & Spear (1982). The estimation of both temperature and pressure has been made using a computer software developed by Reche & Martínez (1996).

Temperatures between 450°C (biotite zone) and 670°C (sillimanite zone) have been obtained. These values are consistent with the temperatures expected from the prograde mineral assemblages present in the pelitic metasediments, which are typical of a low to medium pressure and high temperature metamorphic evolution (greenschist and amphibolite facies).

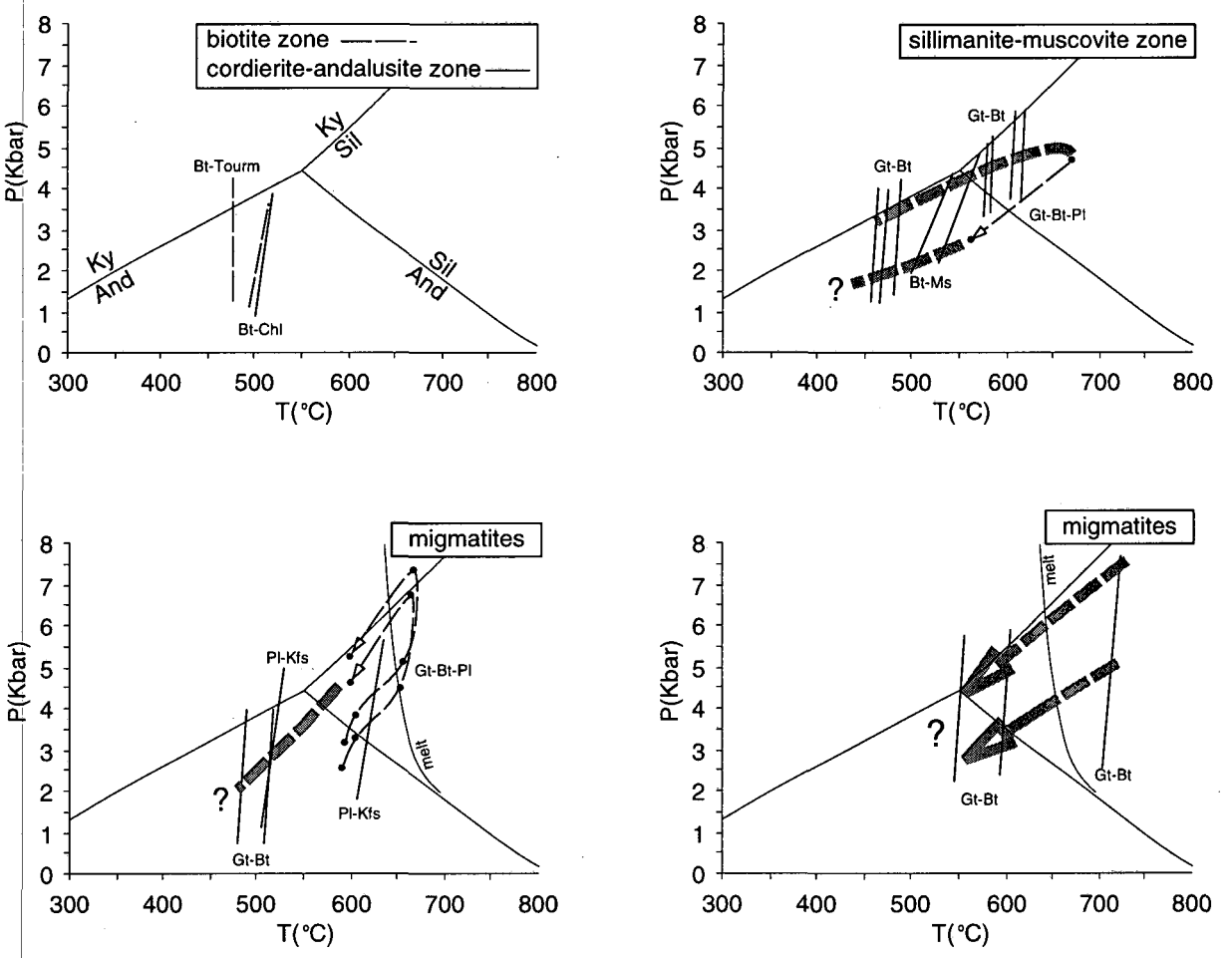

Fig. 31. P-T plots on samples located at different metamorphic zones. Lines correspond to temperature values obtained by geothermometry, slightly varying with pressure. Dots correspond to analyses from cross-sections of garnets from core to rim. Arrows represent the postulated P-T-t paths. Als equilibria have been constructed using the 2.5 ppc version of Thermocalc (Powell & Holland 1988) using most recent thermodynamic database created in June 1996. Melting curve after Grant (1985).

The P-T conditions for the sillimanite zone vary from 670°C and 4.7 Kbar (values corresponding to the core of a garnet with retrograde zoning) to 560°C and 2.4 Kbar (for the rim of the same garnet). The former P-T values might correspond to the approximate peak metamorphic conditions, if we assume that the maximum temperature values are recorded in the core of garnet crystals. These data agree with previous estimations by Reche in BRGM-ITGE (1997). In that case, P-T conditions estimated by a petrogenetic grid approach yielded 600°C and 4.3-4.6 Kbar for the upper part of the cordierite-andalusite zone.

In the Punta dels Farallons migmatite complex, temperatures between above 700°C and 480°C have been obtained by Gt-Bt geothermometry. P-T-t paths may be constructed on the basis of data obtained from garnet migmatites (Fig. 31). These indicate pressures up to 7.4 Kbar. Much quantitative data is needed to verify or discard such high-pressure values in relation to the maximum 4.7 Kbar obtained in the sillimanite zone.

Other pressure and temperature estimates from the Cap de Creus rocks had previously been obtained by other authors, and these have been taken into account in this thesis. These estimates refer mainly to: 1) the pegmatites and 2) the P-T conditions during mylonitization.

1) Temperatures of crystallization of type I pegmatites are estimated to be above 580°C (Alfonso 1995) and about 600°C (Damm et al. 1992). For the most differentiated albite pegmatites, located in the cordierite-andalusite zone, P-T conditions about 550°C and 3 Kbar are indicated by Alfonso (1995).

2) A petrological evolution was established for mylonites from the Cala Serena shear zone (Bossière et al. 1995, 1996). In the protomylonitic samples, the temperature range obtained by the use of a Bt-Gt thermometer is 474°-575°C, whereas in mylonites it is about 430°C, for pressures of some 3 Kbar. The higher values in the less deformed samples are interpreted as being inherited from the previous amphibolite facies metamorphism.

4 THE STRUCTURE

In the next sections, I proceed to the description and interpretation of structures of a polyphase tectonic sequence. The first (D1) event groups early deformations which basically led to the development of a first ubiquitous penetrative schistosity. The last deformations recorded are represented by retrograde folds and shear zones, which overprint all the previous structures. Between these two readily differentiable early and late events, there is a complex tectonic pattern characterized by progressive inhomogeneous deformation. As a consequence of this complex deformational pattern, separation and correlation of different events has been difficult and has required the combined use of several criteria, detailed in section 4.2.

4.1. EARLY DEFORMATIONS

The early deformation, labelled D_1, include the group of structures generated before or during the first stages of the prograde metamorphism. These structures are difficult to characterize due to the effects of later overprinting and to the problem of correlating isolated outcrops where they are recognizable. Two main features evidence the early deformations. First, the presence of an ubiquitous penetrative schistosity (S_1) in almost the entire study area. Second, the lithological maps reveal the possible existence of folds and tectonic slices which could presumably be related to these first events.

4.1.1. PENETRATIVE EARLY DEFORMATION

Structural elements related to D_1 deformation are: the S_1 foliation, the F_1 axial surfaces, the intersection lineation (L_1) between bedding (S_S) and S_1, and the F_1 fold axes.

The S_1 foliation or schistosity is well defined in rocks of the metasedimentary sequence by the alignment of phyllosilicates, and generally consists of an ubiquitous penetrative planar fabric well visible at different scales. It is frequently developed either as a slaty cleavage in fine grained rocks or as a spaced cleavage in coarser greywackes. The D_1 event did also produce deformation structures in the pre-Hercynian igneous rocks (metabasites and Port de la Selva gneisses, the latter developing a typical gneissic foliation). The S_1 foliation cannot be considered as the dominant or pervasive foliation throughout the area (regional foliation), since in some domains it appears transposed by later deformations.

Isoclinal minor F_1 folds have been recognised in some outcrops (Fig. 32a), but generally S_1 is sub-parallel to S_S or transposes the S_S throughout the area. When the S_1 foliation is sub-parallel to bedding, both are often described together as $S_{S/1}$ (Fig. 6b). However, in many cases, there is a difficulty in distinguishing between low and high strain D_1 deformation, despite the substantial differences which that would imply. D_1-related boudins and rods affecting the more competent layers are very common (like the interbedded plagioclase-amphibole rocks (Fig. 32b) or the calc-silicate rocks, marbles, gneisses and amphibolites of the Sant Baldiri complex).

The L_1 intersection lineation has a rather constant attitude in areas of uniform S_1 orientation. The mean value for L_1 intersection lineation in the southern and central domains plunges to the ESE (Fig. 33). However, some dispersion of L_1 along rather homogeneously oriented S_1 surfaces has been observed in specific sub-areas (Codera, Mas d'en Duran-S'Alqueria, Map of Structural Domains), where plunges range from NE to SE directed. That could be interpreted as the existence of pre-S_1 folding, a possibility that will be discussed below.

Numerous quartz veins (of millimetric to centimetric width) of D_1 age or older are present in all domains. That means that an incipient metamorphism, involving dehydration reactions, was already present before the D_1 deformation. Many quartz veins were deformed during D_1 and developed S_1-parallel boudins (Fig. 32c) and a stretching lineation in various orientations.

In domains of low post-D_1 overprinting (i.e. where S_1 is the dominant foliation), the present attitude of the S_1 foliation varies slightly between a general NW-SE trend, with moderate to steep NE dips, and a sub-vertical NE-SW trend, especially in the eastern domains around the east coast. Towards the west, the S_1 foliation moderately dips towards the ENE, whereas in the southwesternmost domain has a sub-horizontal attitude (Structural Map, Map of Structural Domains). In the domains located to the NNW, the S_1 foliation appears entirely transposed by later crenulation foliations.

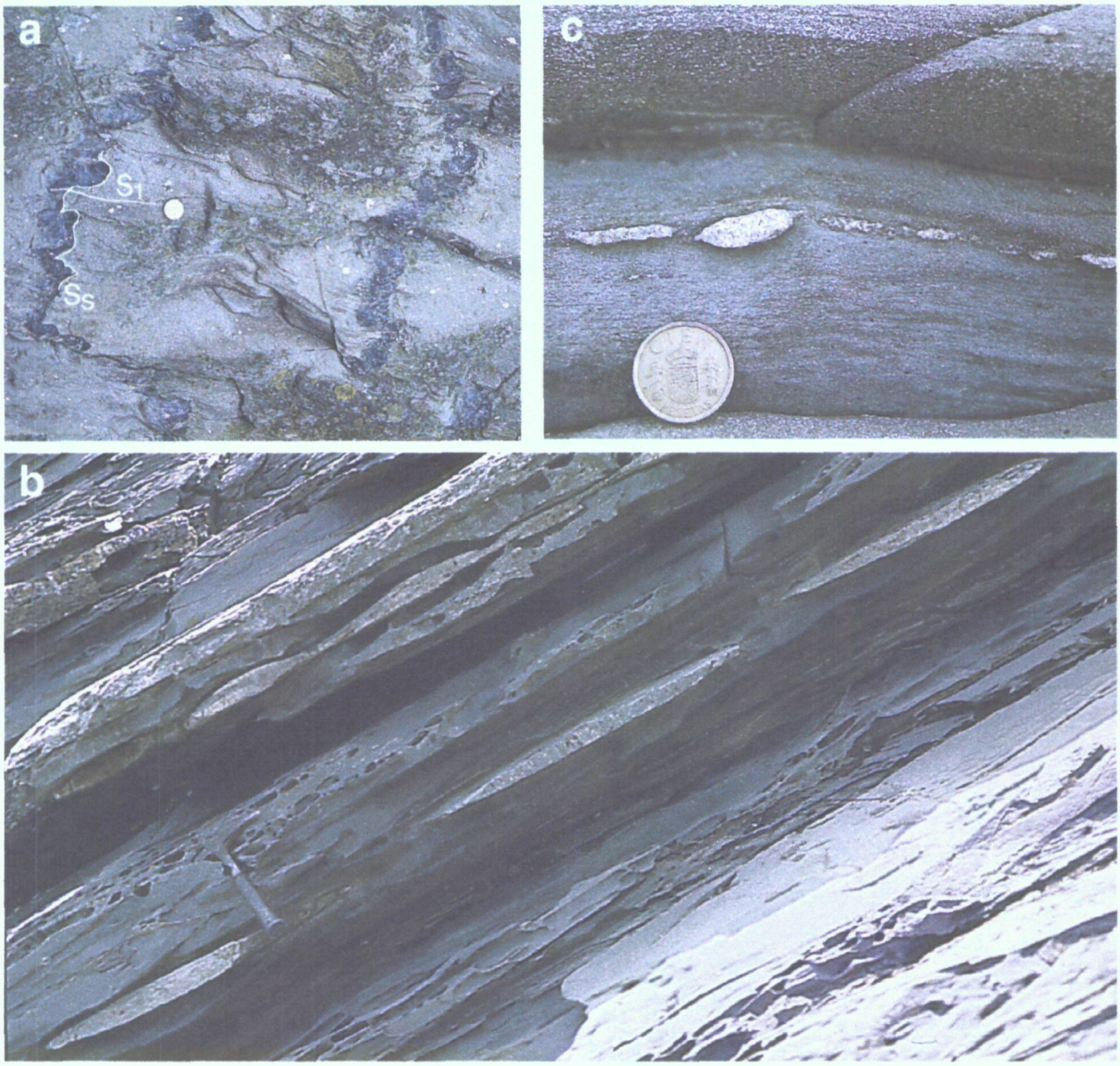

Fig. 32. Field photographs of early structures. (a): F_1 folds affecting bedding (S_S), Cadaqués village. (b): Boudins of plagioclase-amphibole rocks, S'Alqueria. (c): Boudins of S_1-parallel quartz veins, western coast of Cala Jugadora.

Microstructures

The S_1 foliation is mainly developed as a slaty cleavage defined by a good parallel orientation of most minerals. The phyllosilicates have a shape and lattice preferred orientation. (Fig. 34a). As a result of the presence of stacks of mica and chlorite crystals around flat quartz grains, this cleavage may adopt a slightly anastomosing appearance. In most cases, the S_1 cleavage develops parallel to the bedding surfaces, and this is most visible at microscopical scale in finely laminated ritmites (Fig. 34b). However, in some cases, S_1 foliation is oblique to bedding and takes the form of a crenulation cleavage affecting a finely laminated sedimentary fabric (Fig. 34c).

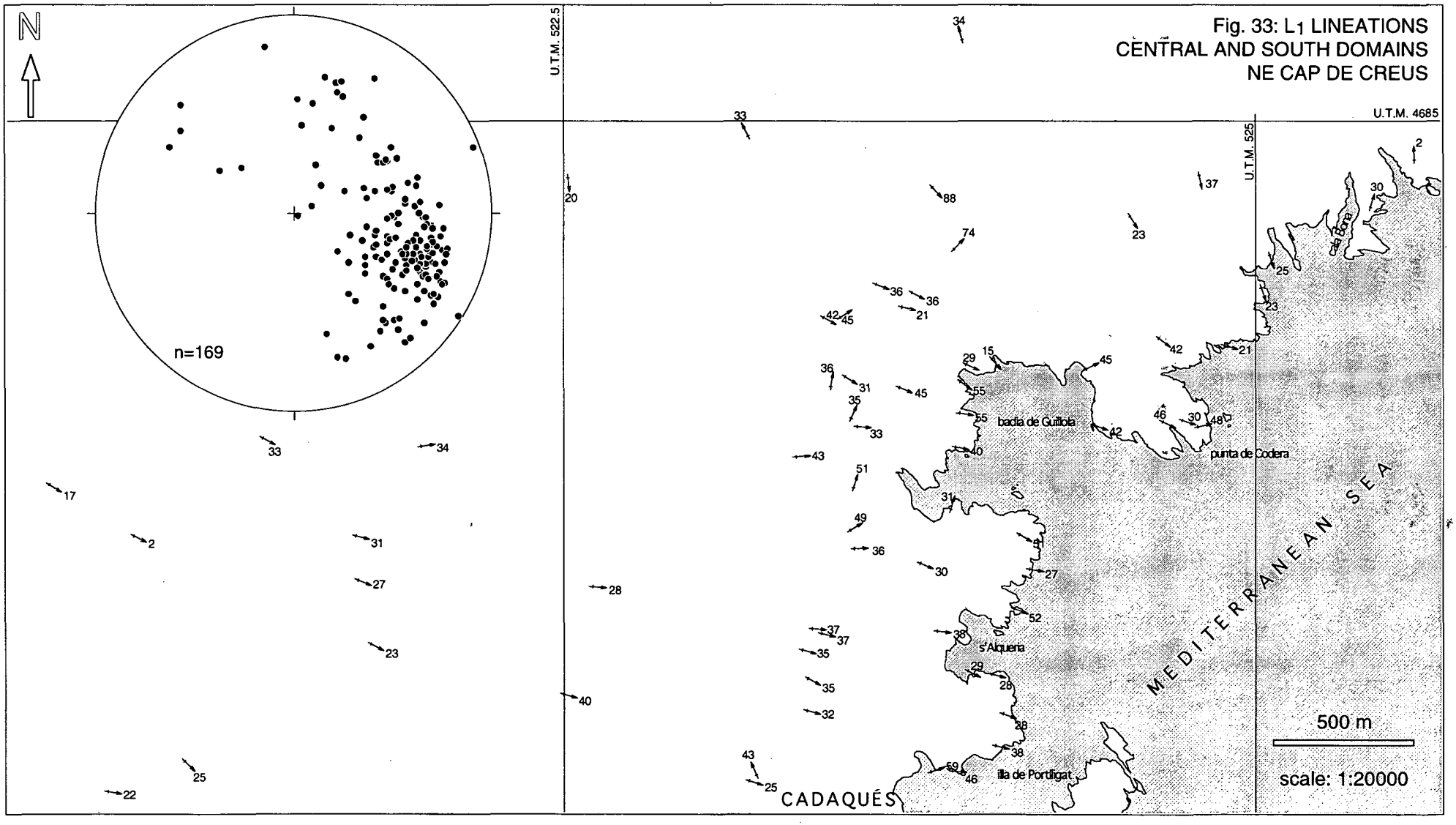
N
n=169
U.T.M. 522.5
U.T.M. 525
U.T.M. 4685
Fig. 33: L1 LINEATIONS
CENTRAL AND SOUTH DOMAINS
NE CAP DE CREUS
cap Gros
badia de Guillola
punta de Codera
s'Alqueria
illa de Portlligat
CADAQUÉS
MEDITERRANEAN SEA
500 m
scale: 1:20000

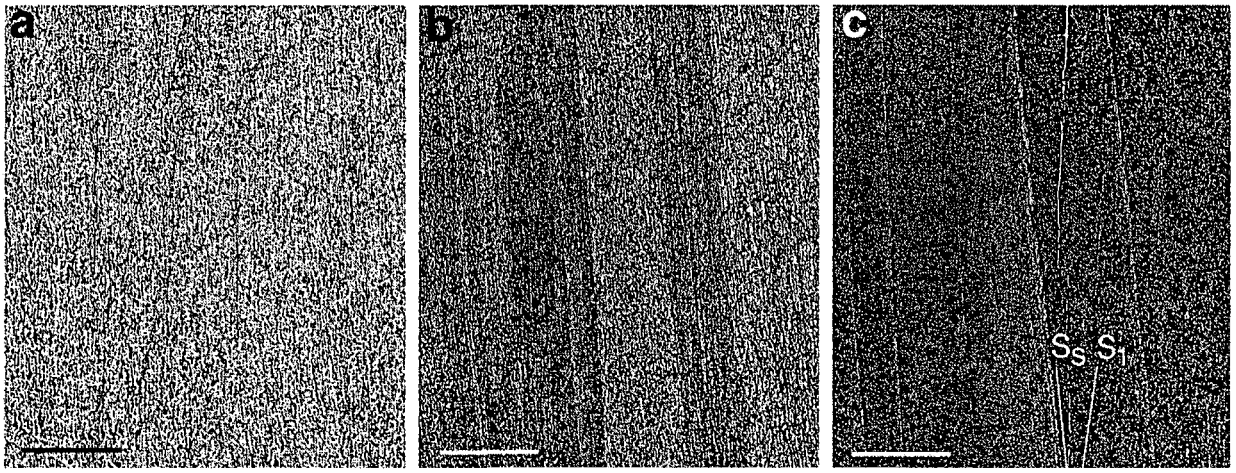

Fig.34. Photographs of D1 microstructures. Scale bar = 2.5 mm. (a) Medium grade schist displaying S_1 foliation. (b) Bedding-parallel S_1 foliation in a metapelite-metapsammite alternance. (c) Bedding-oblique S_1 foliation in very low grade metasediments.

4.1.2. OTHER EVIDENCE OF EARLY TECTONICS

Some beds, layers and sedimentary associations have been used as tracers for large scale structures. Most commonly, they are the Sant Baldiri complex and the quartzite layers. Their distribution in map view is shown in Fig. 5. The rocks of the Sant Baldiri complex are best developed in the western domains, whereas the quartzite layers are widespread in the central and eastern parts of the study area.

As introduced above, in the section explaining the metasedimentary sequence, the Sant Baldiri complex could represent slices of material from the Montjoi and Upper Series pinched in between the metasediments of the lower Cadaqués-Cap de Creus Series. The fact the the S_1 foliation affects uniformly this complex and the series above and below, indicates that these slices were already intercalated at the end of S_1 foliation development. The slices could either represent pinched synforms and/or thrust structures. That might imply synformal structures and/or a contractional fault system involving the rocks of both series. In most of the examples, the S_1 schistosity homogeneously affects the entire set, looking as if the "emplacement" of the Sant Baldiri complex was earlier or contemporaneous to the D_1 deformation. Moreover, the rusty schists adjacent to the Sant Baldiri complex, might represent thrust-related fault rocks. Therefore, a complex pattern of folds and thrust faults might have been operating during the early stages of deformation, and culminating with the development of the penetrative S_1 foliation.

As far as the quartzites are concerned, in principle they seem to be in stratigraphic continuity with other rocks of the sedimentary sequence, and they display minor isoclinal F_1 folds. This is the case, for instance, of an individual quartzite bed (Rabassers quartzite) which crops out with minor interruptions from the Es Jonquet inlet as far as the northward side of Mas Rabassers de Dalt (Structural Map). On the other hand, in more easterly domains, several quartzite beds (up to seven) are displayed between decametric packets of metasediments, and they are always parallel to each other and to the adjacent $S_{S/1}$ surfaces in the metasediments. This is the case of the outcrops comprised between Puig de Culip and Illa de Cullaró, and also between the northern side of Guillola and Rabassers de Baix (Structural Map). The succession of quartzite layers observed in the maps from these areas could represent repetitions due to early tectonics, either by isoclinal folding, by thrusting or by both, with the axial planes and/or thrust surfaces in close parallelism to the S_1 foliation. These structures could be correlatable with those described for the Sant Baldiri complex.

In conclusion, the most unequivocal evidence for early Hercynian deformation in the study area is the presence of the S_1 penetrative foliation and related minor structures. The original orientation of the S_1 foliation and the precise significance of D_1

deformation are difficult of establish in view of the available data. However, if we consider the present S_1 attitude in domains of low post-D_1 strains to be the one most closer to its original disposition, original orientations close to N-S and dipping to the east may be deduced.

There are some indications for the presence of pre-D_1 deformation. The bedding surfaces were not horizontal at the beginning of D_1 event, as shown by plunging L_1 intersection lineations (Fig. 33). A rough approximation gives a possible orientation of the bedding surfaces before D_1 close to NNW-SSE, dipping to the E, on the basis of assimilating the present mean disposition of bedding (i.e. layers of quartzite) in very low strained zones. In such zones where it is possible to recognize bedding, a few stratigraphic way-up indicators have been recorded, showing younging direction to the east. In addition to the locally observed dispersion of the L_1 intersection lineation in areas of homogeneous attitude of the S_1 foliation, a more general survey on the Cap de Creus peninsula also shows original dispersions of L_1 (with a prevalent trend close to SSE), which were interpreted as the result of the existence of pre-D_1 structures (Carreras 1973). The time gap between the pre-D_1 and the D_1 deformational events is not easy to presume. In this context, the possible thrust and associated fold structures that caused the emplacement of the Sant Baldiri complex and the repetitions of the quartzites, are more likely to be closer in time to the D_1 event.

4.2. POST D_1 STRUCTURAL ZONATION AS A RESULT OF COMPLEX SPACE-TIME HISTORY

The study area will be presented in the next sections as a case study of a complex structure resulting from a progressive, inhomogeneous non-coaxial deformation. In such a progressive deformation, different tectonic phases or events are difficult of distinguish. However, for the sake of easy understanding, I have tried to elaborate a systematic view based on the differentiation of deformation events (Fig. 35). In spite of the difficulties, progressive deformations have been grouped and dated relative to one another with the aid of: (i) changes in the tectonic style (in the sense of Turner & Weiss 1963, p. 79); (ii) the proximity of a given foliation to the assumed original spatial orientations of different structures; (iii) the metamorphic conditions at which structures have been developed and (iv) the use of overprinting criteria; as long as the limitations of these methods (e.g. Williams 1985) are kept in mind. Sketches in Fig. 35 roughly represent three different stages in the structural evolution of the area. This means that between the first and the third stages deformation was more or less continuous, without any regional time or interkinematic discontinuity.

Pre-D_2 macrostructure

Before the onset of the deformations labelled as D_2, the S_1 foliation had a variable attitude, reflecting, in the study area, a half-dome shaped macrostructure (Fig. 36). This macrostructure is inferred from changes in orientation of the S_1 foliation, and for the dispersion of the main F_2 and F_3 fold axes across approximately E-W sections transecting central and southern zones of S_1 dominant foliation (Map of Structural Domains and (Fig. 37)). The structural elements (S_1 and fold axes) are steeper towards the east. The existence of a NNW-SSE trending major dome-shaped structure controlling the attitude of later structures was already evidenced in Carreras (1973) and attributed to the so called intermediate phase. However this author evidenced the effects of this structure exclusively on the subsequent late phases, but he did not recognize its existence prior to the D_2 event. The D_2 prograde deformational event, recognized in the present work, does not explain the flexure of early foliation either, so that a pre-D_2 macrostructure should have

existed. However, neither penetrative foliations nor minor structures related to such a macrostructure have been recognized.

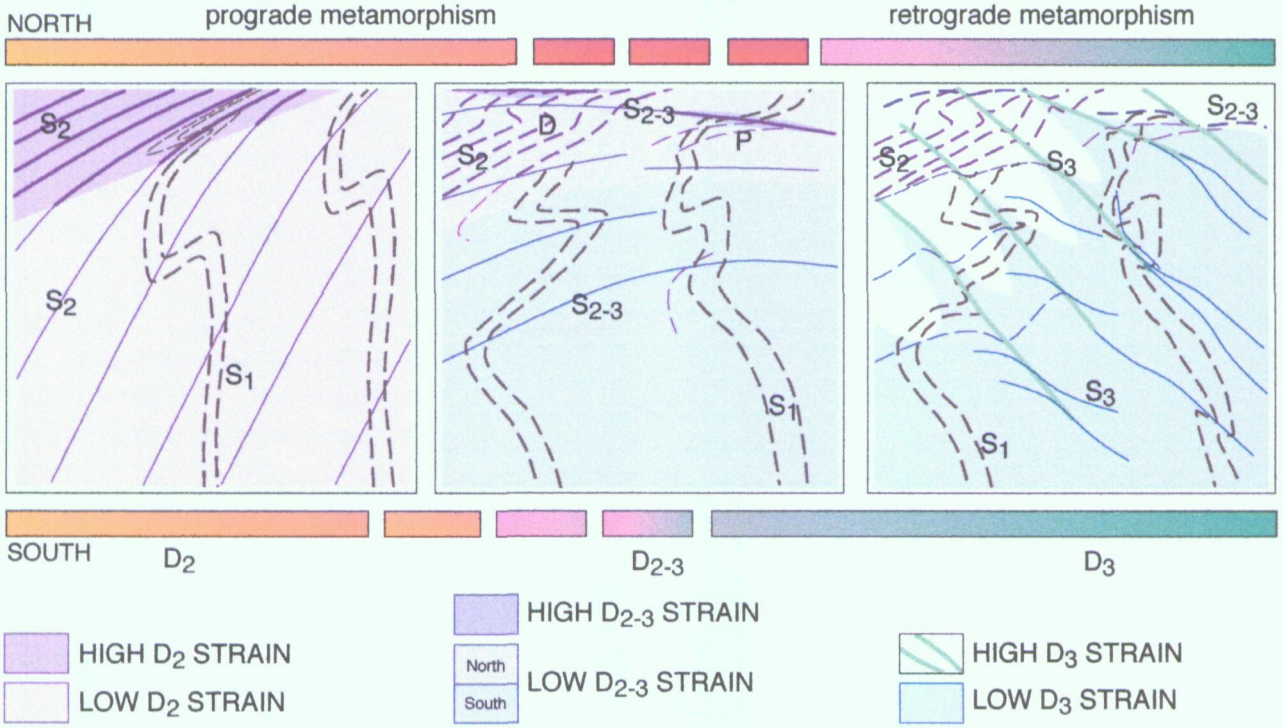

Fig. 35. Conceptual sketches representing three stages in the structural evolution of the area. Thick lines represent the prevalent foliations at each stage. Solid lines represent developing foliations and dashed lines are foliations being deformed. P=progressive deformation, D=discontinuous deformation. D_2 deformation takes place during the prograde metamorphism and D_3 deformations do it at retrograde conditions. An intermediate stage between D_2 and D_3 have different space correlations to metamorphism: while in the north it develops just before and after peak metamorphism conditions, in central and southern domains it develops at more clear retrograde conditions.

The D_2 event, defined as a prograde folding event and explained in detail in section 4.3, is characterized by the folding of the S_1 first schistosity in prograde metamorphic conditions. D_2 structures are controlled by the existence of the S_1 geometry, described above. The prevalent original trend of these structures is close to NE-SW. The existence of fold-related strain gradients across the area enables one to distinguish between structural domains with relatively high and low strain. In general, two main structurally homogeneous domains related to D_2 folding event can be differentiated, a southern low strain domain with a dominating S_1 foliation and a northern high strain domain where S_2 dominates, giving rise to a structural zonation (Map of Structural Domains). This is also shown in Fig. 35, where an ideal surface separating domains of low and high D_2 strain is shown. In a closer view, second-order inhomogeneities are responsible for the presence, in the low strain domain, of narrow bands marked by tight F_2 folds and, in the high strain domain, of lozenge-shaped zones of minor deformation.

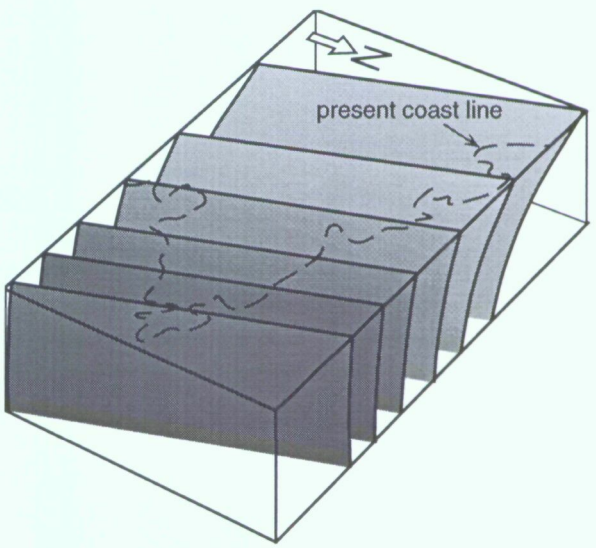

Fig. 36. Three-dimensional sketch showing the possible arrangement of the S_1 foliation before the onset of D_2.

Fig. 37: L_2, L_{2-3} AND L_3 LINEATIONS NE CAP DE CREUS PENINSULA

U.T.M. 522.5

U.T.M. 525

U.T.M. 4687.5

U.T.M. 4685

N

1 km

scale: 1:20000

21 L_3 mylonite stretching lineations

57 L_{2-3} lineations and fold axes in low and medium grade metamorphic rocks; L_3 lineations and fold axes

59 L_{2-3} lineations and fold axes in high grade metamorphic rocks

48 L_2 lineations and fold axes

The D_2 folding structures evolved to an E-W trend (folds and crenulation cleavages). These deformations have been grouped under the name D_{2-3} E-W folding stage, and will be described in section 4.4. D_{2-3} deformation is also heterogeneous, giving rise to lower and higher strain zones. In the northern area, the D_{2-3} stage is difficult to distinguish from the D_2 event, because the progressive character of deformation and the relative high temperature conditions at which both, D_2 and D_{2-3}, structures were developed. This is particularly manifest in those areas affected by low to medium D_2 strain that have been progressively submitted to D_{2-3} deformation. In some D_2 high strain domains, D_{2-3} structures are relatively much easier to distinguish because overprinting of S_2 surfaces by S_{2-3} folds. On the other hand, in the central and southern domains, these E-W folds were developed at retrograde conditions, being difficult to distinguish from the following D_3 structures. Consequently, D_{2-3} is a way to designate an intermediate transitional stage between D_2 and D_3, comprising structures that may show similarities to either D_2 or to D_3 depending on the metamorphic conditions at which they were developed.

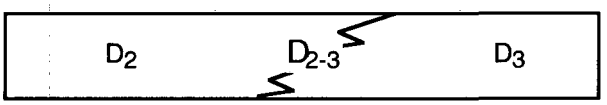

Although the use of this terminology might appear somewhat confusing, it is considered the most adequate approach to describe the complex structural pattern of the area. The need of presenting a D_{2-3} transitional stage will be profusely justified in section 4.4.

There are close relationships between the D_2 and D_{2-3} structural stages and the emplacement of intrusive bodies (granitoids of the migmatite complexes and pegmatite dykes). The structures displayed by the intrusive rocks and by the migmatitic schists provide good evidence for the penecontemporaneity of deformation, magmatism and migmatization. These relationships will be described in detail in a following chapter (sections 5.2. and 5.3.).

The late structure, described in section 4.5, correspond to D_3 folds and shear zones, developed under retrograde metamorphic conditions. Spatial gradual changes in the structural style during this late deformation produced a second structural zonation, evidenced by the disappearance in higher grade domains of late folds and the preponderance of shear zones (Carreras 1975, Carreras & Casas 1987). The prevalent original orientation of the D_3 late folds is close to NW-SE. Interference structures are common where the S_1 foliation is affected by D_2 and D_3 folding. F_3 folds and shear zones set out the boundaries of the present sub-areas (Map of Structural Domains). The resulting lozenge-shaped bodies are function, therefore, of the combined effects of the space-time heterogeneity of deformation and an anastomosing mylonitic framework generated by late shearing.

Westwards from the study area (West of Cala Taballera and around El Port de la Selva), D_2 and D_3 structures trend closely parallel, with an E-W orientation. Consequently, the problem of identifying different structural events is much greater and, for this reason, I have concentrated efforts in the northeastern part of the Cap de Creus penisnula.

4.3. D_2 PROGRADE FOLDING EVENT

The D_2 prograde folding event includes the set of observed structures which formed following the stage when the S_1 foliation was already developed and for a period when prograde regional metamorphism was widespread in the whole area.

This event was responsible for the shaping of a complex folding pattern, characterized by the progressive heterogeneous deformation of a rather homogeneous S_1 foliation (Fig. 38) and, then, by the development of a first structural zonation, with domains of relative high and low strain (Map of Structural Domains).

The formation of F_2 folds and S_2 crenulation cleavage is the prevalent attribute in this set of deformations. Since the lower and the higher strain domains show rather different fold styles, they will be described separately.

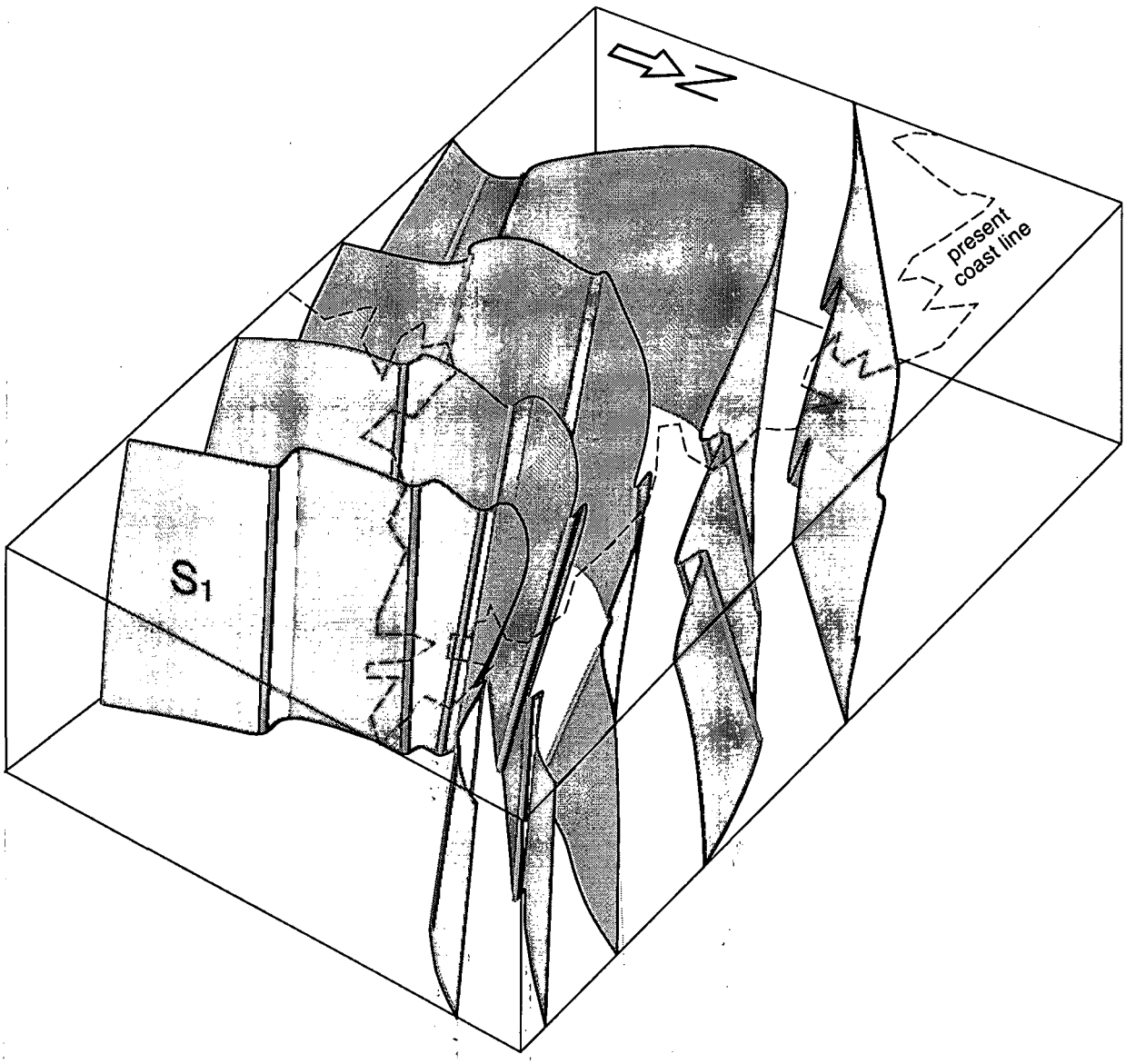

Fig. 38. Three-dimensional sketch of an hypothetical stage after the D_2 folding event, showing the main folding pattern of the S_1 foliation.

4.3.1. STRUCTURES IN THE LOW STRAIN DOMAINS

The low strain domains are characterized by a nearly N-S to NE-SW trend of the $S_{s/1}$ or S_1 foliation (Structural Map and Map of Structural Domains). This foliation is heterogeneously folded into moderately inclined to upright F_2 asymmetrical open folds with moderately plunging to sub-vertical F_2 axes.

Associated to these folds, a D_2 crenulation cleavage develops preferentially in the pelitic schists (Fig. 39a), whereas it is weak or absent in metagreywackes. In the metapelites, crenulations are mainly defined by the preferred orientation of biotite growth in the whole area, and by biotite + sillimanite in the medium to high grade metamorphic zones. D_2 tectonic bandings are rather common in pelitic schists. Porphyroblasts of cordierite, andalusite and garnet are grown over S_1 and often appear rotated with respect to S_1 and towards parallelism with the crenulation cleavage. Those quartz segregation veins which were emplaced prior to the development of F_2 folds (i.e. the earlier boudinaged parallel to S_1 quartz-veins) also rotated during D_2 (Fig. 40). The information given by both the porphyroblasts and the early quartz-veins as kinematic indicators will be discussed in a following section.

The axial planes of the F_2 folds and the S_2 associated axial planar crenulation cleavage trend NE-SW in the less strained domains, showing a clockwise attitude in regard to the nearly N-S S_1 enveloping surface (Structural Map and Map of Structural Domains). Hence, folds show usually an asymmetrical S-shaped geometry (Fig. 39b), which is prevalent at all scales. No major F_2-related reverse limbs have been detected in these lower strain domains.

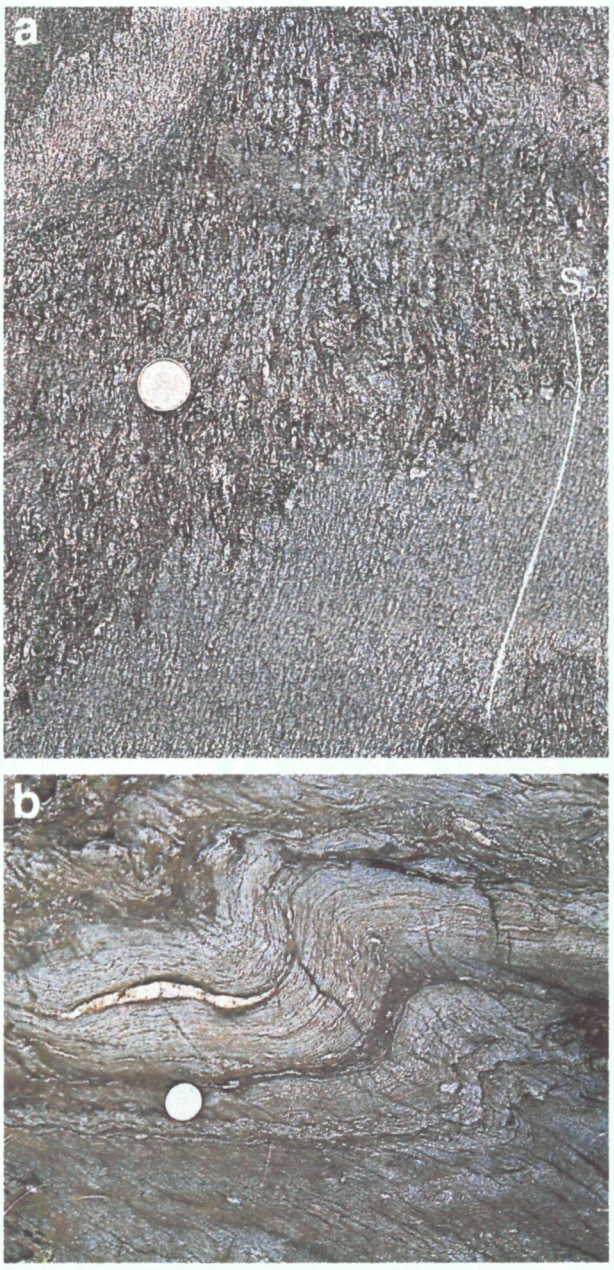

Fig. 39. Field photographs in horizontal view. (a): S_2 crenulation is more developed in metapelites than in metagreywackes, Puig de Culip. (b): F_2 folds in a low strain domain, showing "S"-asymmetry, western coast of Cala Jugadora.

The angle between the mean S_1 orientation and the axial plane crenulation cleavage decreases towards higher strain domains from about 45° (i.e. Puig Alt, cala Torta zone, south Culip area) to 25° or less (i.e. south lighthouse zone). This variation is often accompanied by a simultaneous clockwise rotation of both surfaces. This rotation and the decrease of the angle between the two structural elements might be interpreted as the result of increasing rotational D_2 strain, as shown by the increasing fold tightness. Such angle decrease is observed at different scales, reflecting D_2 strain inhomogeneities, rather than the effects of a later overprinting. In a few places, small deviations of the crenulation cleavage from parallelism with the axial surfaces of the folds give rise to cleavage-transected F_2 folds, indicating once more that D_2 was progressive and non-coaxial.

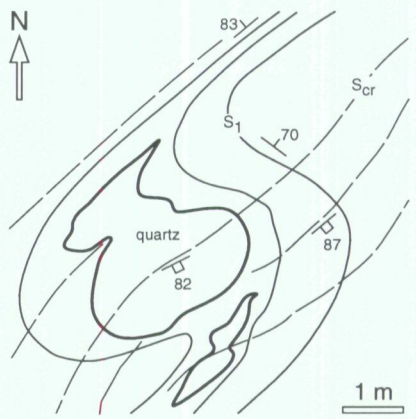

Fig. 40. Field sketch showing the arrangement of structures around a folded early boudinaged quartz vein, Puig de Culip (map view).

The F_2 folds have moderately plunging (in the westernmost areas) to sub-vertical axes (eastwards), which are closely parallel to the L_2 lineations (Fig. 37). L_2 are usually crenulation lineations and mineral lineations defined by biotite or sillimanite (Fig. 41a) and mainly developed in the S_1 foliation and/or in bedding (Fig. 41b). These fold axes and L_2 lineations usually plot near to the fold axes corresponding to the deduced cylindrical folds affecting the S_1 foliation (Map of Structural Domains).